

Chiral splitting of Kondo peak in triangular triple quantum dot

Yi-Ming Liu(刘一铭), Yuan-Dong Wang(王援东), and Jian-Hua Wei(魏建华)
Citation: Chin. Phys. B, 2022, 31 (**5**): 057201. DOI: 10.1088/1674-1056/ac29a5
Journal homepage: http://cpb.iphy.ac.cn; http://iopscience.iop.org/cpb

What follows is a list of articles you may be interested in

Capacitive coupling induced Kondo-Fano interference in side-coupled double quantum dots

Fu-Li Sun(孙复莉), Yuan-Dong Wang(王援东), Jian-Hua Wei(魏建华), Yi-Jing Yan(严以京)
Chin. Phys. B, 2020, 29 (**6**): 067204. DOI: 10.1088/1674-1056/ab8ac1

Electrically tunable spin diode effect in a tunneling junction of quantum dot

Xukai Peng(彭许凯), Zhengzhong Zhang(张正中)
Chin. Phys. B, 2019, 28 (**12**): 127202. DOI: 10.1088/1674-1056/ab53d0

Magnetotransport properties of graphene layers decorated with colloid quantum dots

Ri-Jia Zhu(朱日佳), Yu-Qing Huang(黄雨青), Jia-Yu Li(李佳玉), Ning Kang(康宁), Hong-Qi Xu(徐洪起)
Chin. Phys. B, 2019, 28 (**6**): 067201. DOI: 10.1088/1674-1056/28/6/067201

Direct spin-phonon coupling of spin-flip relaxation in quantum dots

Ji-Wen Yin(尹辑文), Wei-Ping Li(李伟萍), Hong-Juan Li(李红娟), Yi-Fu Yu(于毅夫)
Chin. Phys. B, 2017, 26 (**1**): 017201. DOI: 10.1088/1674-1056/26/1/017201

Decrease of back recombination rate in CdS quantum dots sensitized solar cells using reduced graphene oxide

Ali Badawi
Chin. Phys. B, 2015, 24 (**4**): 047205. DOI: 10.1088/1674-1056/24/4/047205

Chiral splitting of Kondo peak in triangular triple quantum dot

Yi-Ming Liu(刘一铭)[1], Yuan-Dong Wang(王援东)[2], and Jian-Hua Wei(魏建华)[1,†]

[1] *Department of Physics, Renmin University of China, Beijing* 100872, *China*
[2] *School of Electronic, Electrical and Communication Engineering, University of Chinese Academy of Sciences, Beijing* 100049, *China*

(Received 8 July 2021; revised manuscript received 2 September 2021; accepted manuscript online 24 September 2021)

New characteristics of the Kondo effect, arising from spin chirality induced by the Berry phase in the equilibrium state, are investigated. The analysis is based on the hierarchical equations of motion (HEOM) approach in a triangular triple quantum-dot (TTQD) structure. In the absence of magnetic field, TTQD has four-fold degenerate chiral ground states with degenerate spin chirality. When a perpendicular magnetic field is applied, the chiral interaction is induced by the magnetic flux threading through TTQD and the four-fold degenerate states split into two chiral state pairs. The chiral excited states manifest as chiral splitting of the Kondo peak in the spectral function. The theoretical analysis is confirmed by the numerical computations. Furthermore, under a Zeeman magnetic field B, the chiral Kondo peak splits into four peaks, owing to the splitting of spin freedom. The influence of spin chirality on the Kondo effect signifies an important role of the phase factor. This work provides insight into the quantum transport of strongly correlated electronic systems.

Keywords: Kondo effect, quantum dot, chiral splitting

PACS: 72.15.Qm, 73.21.La, 73.23.–b **DOI:** 10.1088/1674-1056/ac29a5

1. Introduction

As discussed by Berry,[1] the wave function acquires geometric phase, Berry's phase, when it is adiabatically moves along a circuit in the Hamiltonian parament space. In metallic magnets, a complex factor occurs when electrons hop along the noncoplanar spin configurations, resulting in spin chirality.[2] The phase is the vector potential generated by electron spins, and corresponds to the Berry phase experienced by hopping electrons. Consider an electron hopping along a loop $1 \to 2 \to 3 \to 1$, the total phase acquired by the electron is the solid angle subtended by the three spins $\boldsymbol{S}_i$ $(i = 1,2,3)$ and is proportional to the spin chirality $\boldsymbol{S}_1 \cdot (\boldsymbol{S}_2 \times \boldsymbol{S}_3)$. Such a gauge flux acts as a fictitious magnetic field and affects the charge dynamics as the real magnetic field, which is an important physical phenomenon in strongly correlated electronic systems.[3–6]

The Kondo effect[7] reflects the low energy many-body correlation of electrons, which describes the local moment screening of an isolated electron by the itinerant electrons via an antiferromagnetic interaction at low temperatures; which has been the core of theoretical and experimental investigations for several decades,[8] especially the experimentally observed Kondo effect in nanostructures[9–11] and theoretical studies in magnetic field.[12] Moreover, quantum dot devices are particularly suitable for studying the Kondo effect owing to the strong operability. Especially the triple quantum-dot system, which present various Kondo effects depending on magnetic field,[13,14] electron filling $N_{\rm tot}$,[15,16] quantum phase transition,[17–19] and low-energy electronic transport properties.[20–28]

In a ring-like TTQD structure, spin chirality is induced by the noncoplanar spin configuration. Existing studies show spin chirality has been applied to quantum computation by spin cluster qubits[29,30] in TTQD system. In addition, the spin Berry phase has profound significance in gauge theory of strongly correlated electronic systems. For example, the anomalous Hall effect (AHE) observed in colossal magnetoresistance manganites is a manifestation of the Berry phase effect, which is caused by carrier hopping within a nontrivial spin background;[31] and the one that bias-induced chiral current in TTQD system.[32] This makes a difference by considering spin chirality as a new factor in TTQD system. Therefore, the spin chirality entangling with Kondo effect at low temperature is expected to induce nontrivial physical phenomenona. Insight by the above developments, we investigate the influence of spin charity on Kondo effect in TTQD system.

The TTQDs structure comprise three triangularly configured and coupled quantum dots with one dot (defined as QD1) connected to one electron reservoir. Three quantum dots are coupled through tunneling strength t with single occupation on each dot (Fig. 1). The Hamiltonian of TTQD is described by Anderson impurity model. In absence of external field and electron reservoir, the spin alignment is coplanar, so spin chirality is degenerate. The four-fold degenerate chiral states $|q\rangle$ comprise the ground states of isolated TTQD. At same time, the Kondo screening occurs between QD1 and itinerant electrons of noninteracting electron reservoir via an antiferromagnetic interaction in the equilibrium state at low temperature. A corresponding Kondo peak appears around $A_1(\omega = 0)$ (Fig. 2(b)) in the spectral function of QD1, which is attributed

†Corresponding author. E-mail: wjh@ruc.edu.cn

© 2022 Chinese Physical Society and IOP Publishing Ltd

to electrons tunneling between four-fold chiral ground states, one is induced by virtual processes of the excited state. As tunneling strength t increases, the Kondo peak splits into bimodal peaks with a split space of $3/2J$ ($J \sim 4t^2/U$), indicating t-induced antiferromagnetic interaction J. Analogous Kondo peak splitting caused by interdot tunneling t in coupled double quantum dots.[33] Moreover, particle–hole asymmetry appears with increasing tunneling t. We apply a perpendicular magnetic field to restore particle–hole symmetry of TTQD system.

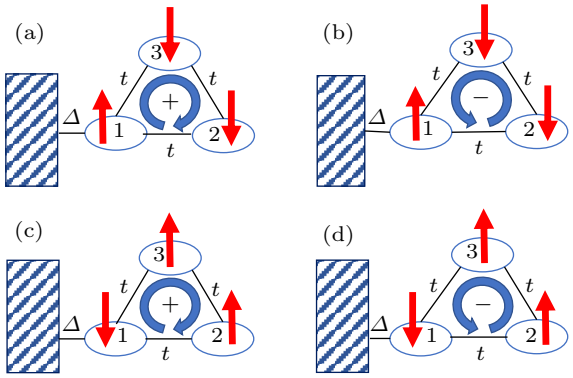


Fig. 1. Geometry of TTQD. The electrons circle around TTQD structure, which generates two equivalent directions of chiral ring current. The sign (+) in black denotes the clockwise direction, (−) represents the anticlockwise direction. QD1 is connected to the electron reservoir by coupling strength $\Delta = 0.5$ meV and the same tunneling strength t between three dots to hold C_{3v} symmetry. Chiral spin states for (a) $|q_+^{-1/2}\rangle$, (b) $|q_-^{-1/2}\rangle$, (c) $|q_+^{1/2}\rangle$, (d) $|q_-^{1/2}\rangle$.

Under perpendicular magnetic field, the virtual current moving around magnetic flux enclosed TTQD loop induces the Berry phase in real space, that is Aharonov–Bohm phase.[34] Existing results show perpendicular magnetic field splits the degeneracy of left- and right-hand chiral states $|q_\pm\rangle$[32,35,36] in TTQD geometry. The chiral interaction induced by the magnetic flux forms a non-coplanar spin texture with spin chirality, leading to chiral splitting of the Kondo peak. The chiral splitting is contributed by the electron hopping between two chiral state pairs $|q_\pm\rangle$, which is produced by phase (φ)-dependent chiral interaction coefficient χ. Numerical calculation results show there has a linear relationship between the space of splitting chiral Kondo peak and chiral interaction coefficient χ. Furthermore, when applied Zeeman magnetic field B as well as perpendicular magnetic field, chiral Kondo peaks split into four peaks owing to B lifts the degeneracy of spin freedom. Quantum fluctuations between both spin and chiral orbital degrees of freedom cause an exotic SU(4) Kondo effect at low temperatures, which manifests as four-peak splitting. A similar SU(4) Kondo effect has been reported in carbon nanotubes.[37,38] The influence of spin chirality on the Kondo effect indicates a core role of the phase factor in TTQD system. Some studies show the phase is a key factor effect on the bias-induced chiral current[32] as well as chirality-based coded qubit in TTQD,[30] while the spin chirality produced by phase further effect on the Kondo effect is seldom studied in TTQD system. Such innovation of the Kondo physics motivates us to study a triangular triple quantum dot (TTQD) as the simplest multiple QD system with a closed loop. This work indicates the phase factor under magnetic field introduces new features into low energy quantum transport in strong correlated systems and the numerical results provide a detailed understanding of physical characters for the implementation in experiment.

2. Model and methods

A schematic diagram in Fig. 1 shows one electron on each dot; therefore, spin $= 1/2$. The total Hamiltonian is $H_{\rm T} = H_{\rm dots} + H_{\rm res} + H_{\rm coup}$, which can be described by the Anderson impurity model

$$H_{\rm dots} = \sum_{i,j=1}^{3} \sum_{\mu=\uparrow,\downarrow} t_{ij} d_{i\mu}^{\dagger} d_{j\mu} + \sum_{i=1}^{3} U_i n_{i\uparrow} n_{i\downarrow}, \tag{1}$$

here, $\varepsilon_i = t_{ii} = -U_i/2 = -U/2$, where ε_i and U_i are the on-site energy and the Coulomb repulsion of i-th dot, respectively; μ is the electron spin orientation, i.e., $\mu = \uparrow$ or $\mu = \downarrow$. $n_{i\mu} = d_{i\mu}^{\dagger} d_{i\mu}$ is the operator of the occupation number on the i-th dot and t_{ij} is the hopping matrix between i-th and j-th dots, with $t_{12} = t_{23} = t_{31} = t$ to hold the C_{3v} symmetry.

The noninteracting electron reservoir is $H_{\rm res} = \sum_{\alpha k\mu} \varepsilon_{\alpha k\mu} c_{\alpha k\mu}^{\dagger} c_{\alpha k\mu}$, where $\varepsilon_{\alpha k\mu}$ is the single particle energy level of the $|k\rangle$ state with μ spin for α electrode, $c_{\alpha k\mu}^{\dagger}$ and $c_{\alpha k\mu}$ are the corresponding creation and annihilation operators of the reservoir electrons. The coupling between electron reservoir and quantum dots is $H_{\rm coup} = \sum_{\alpha k\mu} V_{\alpha\mu k}(d_{\mu}^{\dagger} c_{\alpha k} + {\rm H.c.})$, $V_{\alpha\mu k}$ is the tunnel matrix element between imparity electrons and reservoir electrons for the α-reservoir state $|k\rangle$. The effect of electron reservoirs on the dots is taken into account through the hybridization functions, $\Delta_{\mu\nu}(\omega) \equiv \Sigma_\alpha \Delta_{\alpha\mu\nu}(\omega) = \pi \Sigma_{\alpha k} V_{\alpha\mu k}(\omega) V_{\alpha\nu k}^{*}(\omega) \delta(\omega - \varepsilon_{\alpha k})$, with absence of applied chemical potentials. Generally, we adopt Lorentzian hybridization functions in HEOM approch, $\Delta_{\mu\nu}(\omega) = \delta_{\mu\nu} \Delta W^2/(\omega^2 + W^2)$, with Δ being the effective dot–reservoir coupling strength and W is bandwidth of the electrode. The TTQD paraments are $\varepsilon_i = 1.0$ meV and $U = -2\varepsilon_i = 2.0$ meV, the temperature is $k_{\rm B}T = 0.02$ meV, the bandwidth is $W = 5.0$ meV and $\Delta = 0.5$ meV.

The HEOM approach investigates the properties of quantum dots in both equilibrium and non-equilibrium states via the reduced density operator, which has a universal formalism for an arbitrary system Hamiltonian; thus, it can be used to accurately solve the three-impurity Anderson model. The detailed derivation for the HEOM approach is shown in Appendix A and Refs. [39,40], and the final form can be reduced to the following compact form:

$$\dot{\rho}_{j_1\cdots j_n}^{(n)} = -\left(\mathrm{i}\mathcal{L} + \sum_{r=1}^{n} \gamma_{j_r}\right) \rho_{j_1\cdots j_n}^{(n)} - \mathrm{i} \sum_{j} \mathcal{A}_{\bar{j}} \rho_{j_1\cdots j_n j}^{(n+1)}$$

$$-\mathrm{i}\sum_{r=1}^{n}(-)^{n-r}\mathcal{C}_{j_r}\rho^{(n-1)}_{j_1\cdots j_{r-1}j_{r+1}\cdots j_n}. \tag{2}$$

The $\{\rho_{j_1\cdots j_n}(t)^n; n=1,\ldots,L\}$ are auxiliary density matrices, with L denoting the truncation level. The transient current through α-reservoir is read as $I_\alpha(t) = \mathrm{i}\sum_{\mu s}\mathrm{tr}_{\rm sys}[\rho^\dagger_{\alpha\mu s}(t)\hat{d}_{us} - \hat{d}^\dagger_{\mu s}\rho^-_{\alpha\mu s}(t)]$, with $\rho^\dagger_{\alpha\mu s} = (\rho^-_{\alpha\mu s})^\dagger$; the first-tier auxiliary density operators (ADOs) are obtained by solving Eq. (2). Moreover, the spectral density function for i-th QD with μ-spin can be written as

$$A_{i\mu}(\omega) = \frac{1}{\pi}\mathrm{Re}\left\{\int_0^\infty \mathrm{d}t\{C_{a_{i\mu}a^\dagger_{i\mu}}(t) + [C_{a_{i\mu}a^\dagger_{i\mu}}(t)]^*\}\mathrm{e}^{-\mathrm{i}\omega t}\right\}, \tag{3}$$

and $A_i(\omega) = \Sigma_\mu A_{i\mu}(\omega)$.

The HEOM approach is established based on the Feynman–Vernon influence functional path-integral theory[41] and implemented with Grassmann algebra for fermion dissipations.[42] Basically, the HEOM approach is a non-perturbative method for general quantum systems coupled to reservoir that satisfies Grassmann Gaussian statistics.[42–44] Based on the linear response theory of quantum open systems, it can accurately and efficiently obtain a dynamical observable quantity of strongly correlated quantum impurity systems.[39] In practical calculations, we must minimize the computational expenditure while maintaining the quantitative accuracy. For this purpose, we usually impose a truncation L as the highest tier of the ADOs. This truncation decreases the number of EOMs to match the insufficient calculation capacity, without affecting the nonperturbation characteristic of HEOM. This truncation L is measured by the quantitative convergence at $A(\omega=0)$ when the Kondo effect is considered, usually $L=4$ for most physical cases. However, lower temperatures demand a higher truncation tier and more computing resources to achieved numerical convergence. In recent years, HEOM has been widely used to investigate the Kondo effect and transport properties under equilibrium and non-equilibrium conditions in quantum dot systems.[33,45–48]

3. Results and discussion

When perpendicular magnetic field applied, magnetic flux threads the TTQD structure, the t–J–χ model can be derived by treating t in $H_{\rm dots}$ perturbatively [32,49]

$$\begin{aligned} H_{\rm eff} &= -t(1-n)\sum_{ij,\mu}(d^\dagger_{i\mu}d^\dagger_{j\mu} + \mathrm{H.c.}) \\ &\quad + J\sum_{i<j}\left(\widehat{S}_i\widehat{S}_j - \frac{1}{4}n_in_j\right) + \chi\widehat{S}_1\cdot\left(\widehat{S}_2\times\widehat{S}_3\right), \end{aligned} \tag{4}$$

where n is the average occupation number on each dot. The first term will vanish in the half-filling situation ($n=1$). The second term is the Heisenberg exchange interaction with $J = 4t^2/U$. The last term is a chiral term with chiral operator $\widehat{S}_1\cdot(\widehat{S}_2\times\widehat{S}_3)$,[4] where χ is the chiral interaction with $\chi = 24t^3\sin(2\pi\phi/\phi_0)/U^2$, and ϕ is the magnetic flux enclosed by the TTQD structure. $\phi_0 = hc/e$ is the unit of quantum flux. For simplicity, we let $\varphi = 2\pi\phi/\phi_0$; thus, $\chi = 24t^3\sin(\varphi)/U^2$.

For a system with three spins, there are two sub-spaces; one is a quadruplet state with total spin $S=3/2$. It is expressed by $|Q^{1/2}\rangle = (1/\sqrt{3})(|\uparrow_1\uparrow_2\downarrow_3\rangle + |\uparrow_1\downarrow_2\uparrow_3\rangle + |\downarrow_1\uparrow_2\uparrow_3\rangle)$, and $|Q^{3/2}\rangle = |\uparrow_1\uparrow_2\uparrow_3\rangle$. $|Q^{-1/2}\rangle$ and $|Q^{-3/2}\rangle$ are given by flipping all spin orientations of $|Q^{1/2}\rangle$ and $|Q^{3/2}\rangle$ states, respectively. Another subspace for the total spin $S=1/2$ comprises four-fold degenerate chiral ground states $|q\rangle$, which can be expressed as

$$\begin{aligned} |q^{1/2}_\pm\rangle &= \frac{1}{\sqrt{3}}\Big(|\downarrow_1\uparrow_2\uparrow_3\rangle + \mathrm{e}^{\pm\frac{\mathrm{i}2\pi}{3}}|\uparrow_1\downarrow_2\uparrow_3\rangle \\ &\quad + \mathrm{e}^{\pm\frac{\mathrm{i}4\pi}{3}}|\uparrow_1\uparrow_2\downarrow_3\rangle\Big). \end{aligned} \tag{5}$$

The other two states $|q^{-1/2}_\pm\rangle$ can be obtained by flipping all spins of $|q^{1/2}_\pm\rangle$ states.

Furthermore, when perpendicular magnetic field applied to TTQD, the magnetic flux threads the ring-like structure. The former four-fold degenerate chiral ground states in the total spin-1/2 subspace split into two chiral state pairs owing to the last term in Eq. (4), which are the eigenstates of chiral operator $\widehat{S}_1\cdot(\widehat{S}_2\times\widehat{S}_3)$. One pair is $|q_+\rangle$ and another $|q_+\rangle$ can be obtained by replacing the symbol $(+)$ with symbol $(-)$ in Eq. (5). Here, the symbol $(+)$ denotes the spin circling clockwise, and symbol $(-)$ is the spin circling anticlockwise. The difference in eigenvalues between $|q_+\rangle$ and $|q_-\rangle$ states is $(\sqrt{3}/2)\chi$.

In equilibrium state, the Kondo effect in absence of perpendicular magnetic field is similar to the Kondo peak splitting in double quantum dots;[33] which is a process of J-induced Kondo splitting. Figure 2(a) shows the schematic diagram of the splitting of Kondo peak, which depicts the electron spin flip through virtual state; this is aided by the electron bath, from singlet to triplet. The lateral peaks (denoted as blue dotted line arrow) appear with an increase in tunneling (t)-dependent antiferromagnetic strength J between quantum dots. Theoretically, the difference in eigenvalues between $|Q\rangle$ and $|q\rangle$ is $3J/2$, $J\sim 4t^2/U$. Electron hopping between four-fold ground states $|q\rangle$ and excited states $|Q\rangle$ contributes to lateral peaks in Fig. 2(b). The distance between two splitting Kondo peaks are linear with respect to J [shown in Fig. 2(c)]. And electron hopping between four-fold degenerate states $|q\rangle$ contributes to the prime Kondo peak, which is shown in Fig. 2(b).

Moreover, the prime peaks shown in Fig. 2(b) are shifting left with an increase in tunneling strength t, which indicates that the particle–hole is asymmetric. We apply the particle–hole transition to the Hamiltonian of isolated TTQD in Eq. (1), i.e., $d^\dagger_{n\mu} = \mathrm{e}^{\mathrm{i}\frac{2kn\pi}{3}}h_{n\mu}$ $(k=0,\pm1,\pm2,\ldots)$; $d^\dagger_{n\mu}$ is

the creation operator of the particle for the n-th quantum dot with spin μ, and $h_{n\mu}$ is the hole annihilation operator. The term for $t_{i=j}$ and the second term in Eq. (1) is invariable under the particle–hole transition. The term for $t_{i\neq j}$ is shown as $-t\sum_{n,m,\mu}\left(\mathrm{e}^{\mathrm{i}2k\pi(n-m)/3}h^{\dagger}_{m\mu}h_{n\mu}+\mathrm{e}^{\mathrm{i}2k\pi(m-n)/3}h^{\dagger}_{n\mu}h_{m\mu}\right)$. Then, we compare it with the term for $t_{i\neq j}$ in Eq. (1); it can easily obtain the coefficient $t\mathrm{e}^{\mathrm{i}}\,[2k\pi(n-m)/3]\neq t$. Therefore, the particle–hole is naturally asymmetric in isolated TTQD.

When a flux is added to the hopping term $t_{i\neq j}$ in Eq. (1), i.e., $t\to t\mathrm{e}^{\mathrm{i}\phi/3}$, the $t_{i\neq j}$ term can be rewritten as $-t\sum_{n,m,\mu}\left(\mathrm{e}^{\mathrm{i}[2k\pi(n-m)+\phi]/3}h^{\dagger}_{m\mu}h_{n\mu}+\mathrm{e}^{\mathrm{i}[2k\pi(m-n)-\phi]/3}h^{\dagger}_{n\mu}h_{m\mu}\right)$. To recover the particle–hole symmetry, the corresponding coefficient should be identical, where $-t\mathrm{e}^{\mathrm{i}\,[2k\pi(m-n)-\phi]/3}=t\mathrm{e}^{\mathrm{i}\phi/3}$, $m-n$ is an integer, and $\phi=(\pi/2)+k\pi$. Figure 3(b) verifies the above mentioned derivation by calculating the spectral density functions of QD1 at $\varphi=\pi/2$.

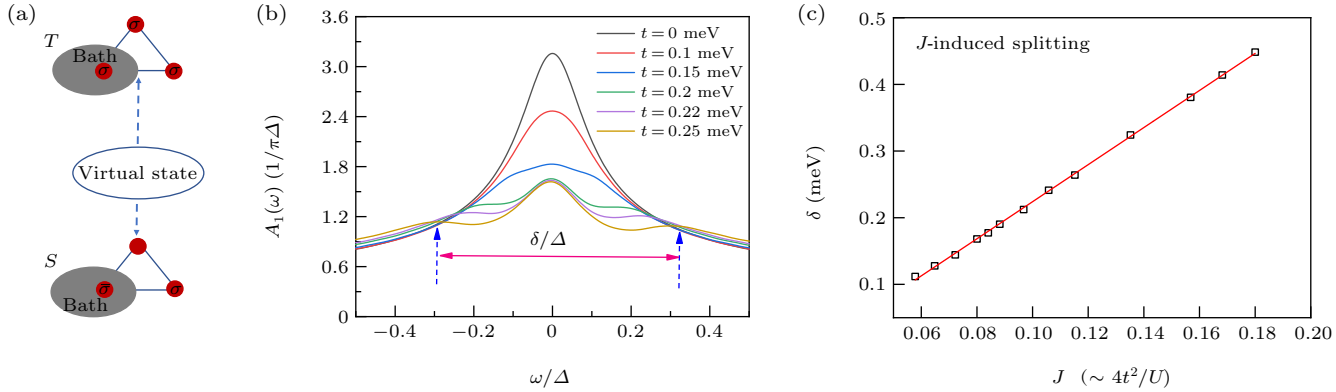


Fig. 2. (a) Schematic diagram of J-induced Kondo peak splitting; electrons in two arbitrary quantum dots participate in the process of Kondo resonance through virtual state; the shadow part is the electron bath and $\sigma=\uparrow$ or $\downarrow$; T denotes the triplet; S is the singlet. (b) Spectral density functions $A(\omega)$ of QD1 with an increasing tunneling strength t without any magnetic field. $A_1(\omega)=2A_{1\uparrow}(\omega)=2A_{1\downarrow}(\omega)$. The blue dotted line arrow points to lateral peaks, and δ/Δ is the distance between two lateral peaks. (c) The scatter combined with the line shows that the space of the two splitting Kondo peaks is exactly linear with respect to J, which is induced by the antiferromagnetic interaction J.

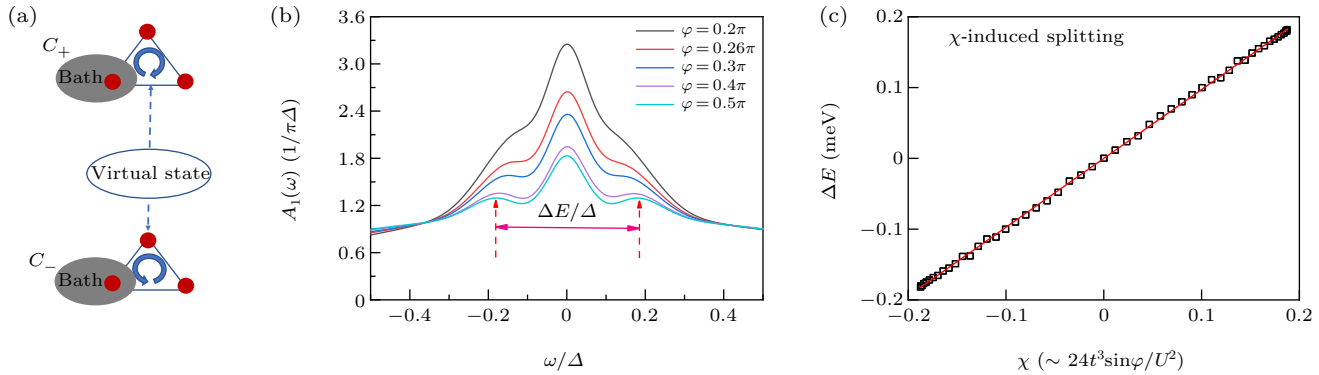


Fig. 3. (a) Schematic diagram of chiral splitting of Kondo peak. C_+ denotes right-hand chiral states $|q_+^{1/2}\rangle/|q_+^{-1/2}\rangle$, and C_- denotes left-hand chiral states $|q_-^{1/2}\rangle/|q_-^{-1/2}\rangle$. The sign of clockwise and anticlockwise arrows corresponds to spin circling directions. (b) Spectral density functions $A(\omega)$ of QD1 with an increasing phase φ under a perpendicular magnetic field. $A_1(\omega)=2A_{1\uparrow}(\omega)=2A_{1\downarrow}(\omega)$. The red dotted line arrow points to two splitting chiral Kondo peaks, the distance between them is $\Delta E/\Delta$. (c) The scatter combined with the line shows that the space of chiral Kondo splitting is exactly linear with respect to χ, which is as function of φ. The TTQD parameter is $t=0.25$ meV.

When a perpendicular magnetic field is applied, a flux ϕ threads the ring like TTQD structure; the correspond phase φ impact on tunneling strength t results a chiral operator $\widehat{S}_1\cdot(\widehat{S}_2\times\widehat{S}_3)$. The chiral operator splits the degeneracy of four-fold ground states into two pairs of chiral states, which are left- and right-hand chiral states. Figure 3(a) shows that the four-fold ground state $|q\rangle$ splits into two chiral state pairs, which are denoted as C_+ (right-hand chiral states) and C_- (left-hand chiral states); but remain the degeneracy of spin freedom. And the transition from C_- to C_+ through virtual state, attributes to splitting of chiral freedoms, i.e., chiral splitting of Kondo peak,which are denoted as C_+ (right-hand chiral states) and C_- (left-hand chiral states); but remain the degeneracy of spin freedom. And the transition from C_- to C_+ through virtual state, attributes to splitting of chiral freedom, i.e., chiral splitting of Kondo peak.

The spectral density functions $A(\omega)$ of QD1 is shown in Fig. 3(b), phase φ increases to $\pi/2$ during quarter period, chiral splitting of the Kondo peak is observed. More computational results exceeding quarter period are detailed in Appendix B. The main peaks in Fig. 3(b) originated from electron hopping between degenerate left-hand chiral state pairs, occupying the $|q_-^{1/2}\rangle$ and $|q_-^{-1/2}\rangle$ states, which gradually lowered with increasing φ. This phenomenon can be explained

by the extension of the lateral peaks with increasing φ. The later peaks (indicated by the arrows flanking the horizonal red dotted line in Fig. 3(b)) are derived from electron hopping between two chiral state pairs, C_- and C_+. The two lateral peaks are separated by $\Delta E/\Delta$, double the difference between the energy levels of the split chiral states pairs.

We extract the numerical computation results about $\Delta E/\Delta$ and compare with theoretical deduction; and find that there is a linear dependence of ΔE on χ, shown in Fig. 3(c), whose slope is 1.94, which is similar to $\sqrt{3}\chi$; the double difference of eigenvalues in theory. That means chiral splitting of Kondo peak is induced by χ. Moreover, since the HEOM approach is an unperturbed method, which considers higher order information, the numerical computation is more accurate. More details can be shown in Appendix B about the comparison of theory and numerical results as a function of the phase φ. The theoretical value χ is deduced by the perturbation method, which involves only a lower order information. By changing phase φ in quarter period, shown in Fig. 3(b), the particle–hole recovers to symmetry at $\varphi = \pi/2$; more numerical computations about the spectral functions as a function of tunneling t at $\varphi = \pi/2$ shown in Appendix B.

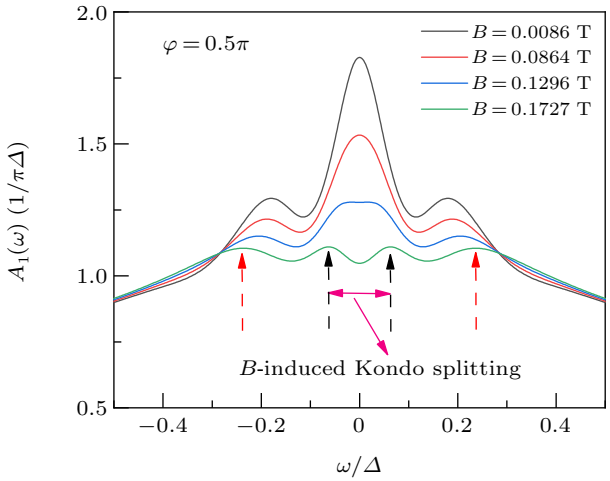


Fig. 4. Spectral density functions $A(\omega)$ of QD1 with increasing Zeeman magnetic field B; $A_1(\omega) = A_{1\uparrow}(\omega) + A_{1\downarrow}(\omega)$. We calculated at $\varphi = \pi/2$ under applied perpendicular magnetic field at $t = 0.25$ meV. The black dotted arrows denote the splitting of spin freedom of Kondo peak, which induced by the Zeeman magnetic field B; the red dotted arrows denote chiral splitting of Kondo peak.

Finally, when transverse magnetic field B applied to the TTQD structure with phase $\varphi = \pi/2$, the chiral Kondo peak still exists at small magnitude B, as shown in Fig. 4; with an increase in B, the chiral Kondo peaks split into four peaks, which is shown in $B = 0.1727$ T. Inter peak (denoted as black dotted line) splitting is induced by B, which means the splitting of spin freedoms of two degenerate chiral state pairs. Analogous situation is the SU(4) Kondo effect observed in carbon nanotubes;[37,38] but the magnetic moment of orbital in carbon nanotubes originate from the two equivalent ways in which electrons can circle around the graphene cylinder; while in TTQD structure, the orbitals stem from the chiral spin states caused by the many-body interactions; and the many-body spin states is closely related to superconductivity.[4] Additionally, the Kondo peak is broken into two peaks with an increase in B without a perpendicular field in Appendix B.

4. Conclusion

In summary, we investigate new characteristic of the Kondo effect caused by the spin chirality arising from the phase factor in the TTQD structure in the equilibrium state. Under a perpendicular magnetic field, a flux φ threads TTQD, lifting the degeneracy of left- and right-hand chiral state pairs $|q_\pm\rangle$. Moreover, the chiral splitting of Kondo peak (Fig. 3(b)) can be explained by electron hopping between two chiral state pairs. The particle–hole revive symmetry by adjusting magnitude of flux $\varphi = \pi/2$. The numerical simulation results in agreement with analytical results (Fig. 3(c)). Furthermore, the Zeeman magnetic field B lifts the spin freedom degeneracy of chiral state pairs, leading to splitting of four peaks (shown in Fig. 4) under perpendicular magnetic field conditions. This work indicates the phase factor plays a core role in introducing new features into Kondo effect in strong correlated systems and the numerical results provide a detailed understanding of physical characters for the implementation in experiment.

Acknowledgments

Computational resources have been provided by the Physical Laboratory of High Performance Computing at Renmin University of China. Project supported by the National Natural Science Foundation of China (Grant Nos. 11774418, 11374363, and 21373191).

Appendix A: HEOM approach

The HEOM approach is established based on Feynman–Vernon influence functional path-integral theory[41] without any approximations, and implemented with Grassmann algebra for fermion dissipations.[42] Basically, the HEOM is a non-perturbative method for general quantum systems coupled to reservoir baths those satisfy Grassmann Gaussian statistics. The reduced density matrix and a set of auxiliary density matrices are the basic variables in HEOM. Basing on the linear response theory of quantum open systems, the HEOM can obtain dynamical observables of strongly correlated quantum impurity systems accurately and efficiently.[39] In recent years, the HEOM approach has been widely used to investigate the Kondo effect and transport properties under equilibrium and non-equilibrium conditions in quantum dots.[33,46,47,50–52,54]

Brief derivation of HEOM approach

At time t, the reduced system density operator, $\rho(t) = \mathrm{tr}_{\mathrm{res}}\rho_{\mathrm{T}}(t)$, is related to the initial value at time t_0 via the reduced Liouville-space propagator $\mathcal{G}(t,t_0)$ by

$$\rho(t) = \mathcal{G}(t,t_0)\rho(t_0). \tag{A1}$$

Let $|\psi\rangle$ be an arbitrary basis set defined in system space, and $\psi = (\psi,\psi')$. Therefore $\rho(\psi,t) = \rho(\psi,\psi',t)$. The operators $f^{\dagger}_{\alpha is}(t)$ are the reservoir operators defined by

$$f^{\dagger}_{\alpha is}(t) \equiv \mathrm{e}^{\mathrm{i}H_{\alpha}t}\left(\sum_{k\in\alpha} V^{*}_{\alpha kis}c^{\dagger}_{\alpha ks}\right)\mathrm{e}^{-\mathrm{i}H_{\alpha}t}, \tag{A2}$$

The influence functional can be evaluated using the Wick theorem and the second-order cumulant expansion method, because all the other higher order cumulants are zero at the thermodynamic Gaussian average for non-interaction leads. As a result, the ensemble average of the second-order cumulants are connected to the reservoir correlation functions $C^{\pm}_{\alpha ijs}(t)$, defined as

$$C^{+}_{\alpha ijs}(t) = \left\langle f^{\dagger}_{\alpha is}(t)f_{\alpha js}(0)\right\rangle_{\mathrm{res}}, \tag{A3}$$

$$C^{-}_{\alpha ijs}(t) = \left\langle f_{\alpha is}(t)f^{\dagger}_{\alpha js}(0)\right\rangle_{\mathrm{res}}, \tag{A4}$$

where $\langle\cdots\rangle_{\mathrm{res}}$ stands for the ensemble average of the reservoirs, and the time translation invariance is used. All LCFs in a form different from that in Eqs. (A3) and (A4) are zero because the lead operators $f^{\dagger}_{\alpha is}(t)$ and $f_{\alpha is}(t)$ satisfy Gaussian statistics. The reservoir spectral density function is defined as

$$J_{\alpha ijs}(\omega) \equiv \frac{1}{2\pi}\int_{-\infty}^{\infty}\mathrm{d}t\mathrm{e}^{\mathrm{i}\omega t}\langle\{f_{\alpha is}(t), f^{\dagger}_{\alpha js}(0)\}\rangle. \tag{A5}$$

For linear coupling with a non-interacting reservoir, the reservoir spectral density function can be evaluated as $J_{\alpha ijs}(\omega) = \sum_k V^{*}_{\alpha kis}V_{\alpha kjs}\delta(\omega-\varepsilon_{\alpha k})$. The auxiliary density operators (ADOs) $\left\{\rho^{n}_{\vec{j}} = \rho_{j_1\cdots j_n}\right\}$ are determined by the time derivative of the influence functional. The final form can be reduced to the following compact form:

$$\begin{aligned}\dot{\rho}^{(n)}_{j_1\cdots j_n} =& -\left(\mathrm{i}\mathcal{L} + \sum_{r=1}^{n}\gamma_{j_r}\right)\rho^{(n)}_{j_1\cdots j_n} - \mathrm{i}\sum_{j}\mathcal{A}_{\bar{j}}\rho^{(n+1)}_{j_1\cdots j_n j}\\ &-\mathrm{i}\sum_{r=1}^{n}(-)^{n-r}\mathcal{C}_{j_r}\rho^{(n-1)}_{j_1\cdots j_{r-1}j_{r+1}\cdots j_n},\end{aligned} \tag{A6}$$

the index $j \equiv (\sigma_{sn})$ corresponds to the transfer of an electron to/from $(\sigma = +/-)$ the impurity state; and the Grassmannian superoperators $\mathcal{A}_{\bar{j}} \equiv \mathcal{A}^{\bar{\sigma}}_{is}$ and $\mathcal{C}_j \equiv \mathcal{C}^{\sigma}_{ijsm}$ are defined via their fermionic actions on an operator $\hat{O}$ as $\mathcal{A}_j\hat{O} \equiv \left[\hat{d}^{\bar{\sigma}}_{is},\hat{O}\right]$ and $\mathcal{C}_j\hat{O} \equiv \eta_j\hat{d}^{\sigma}_{is}\hat{O} + \eta^{*}_j\hat{O}\hat{d}^{\sigma}_{is}$, respectively. The on-dot electron interactions are contained in the Liouvillian of impurities, $\mathcal{L}\cdot \equiv [H_{\mathrm{dot}},\cdot]$. Here, $\rho_0(t) = \rho(t) = \mathrm{tr}_{\mathrm{res}}\rho_{\mathrm{total}}(t)$ is the reduced density matrix and $\left\{\rho_{j_1\cdots j_n}(t)^n; n = 1,\ldots,L\right\}$ are auxiliary density matrices, with L denoting the truncation level. The influence of the α-reservoir can be characterized completely by the hybridization function $J_{\alpha uvs}(\omega) \equiv \pi\sum_{ks}t_{\alpha kus}t^{*}_{\alpha kvs}\delta(\omega-\varepsilon_{\alpha ks})$. The function is assumed to have a Lorentzian form here. In other words,

$$J_{\alpha uvs}(\omega) = \delta_{uv}\delta_{u1}\frac{\Delta_{\alpha}W^2}{(\omega-\mu_{\alpha})^2+W^2}, \tag{A7}$$

with bandwidth W and chemical potential μ_{α}. Moreover, the spectral density function for i-th QD with μ-spin can be written as

$$\begin{aligned}&A_{i\mu}(\omega)\\ &= \frac{1}{\pi}\mathrm{Re}\left\{\int_0^{\infty}\mathrm{d}t\left\{C_{a_{i\mu}a^{\dagger}_{i\mu}}(t) + \left[C_{a_{i\mu}a^{\dagger}_{i\mu}}(t)\right]^{*}\right\}\mathrm{e}^{-\mathrm{i}\omega t}\right\},\end{aligned} \tag{A8}$$

and $A(\omega) = \Sigma_{i\mu}A_{i\mu}(\omega)$.

Comments on the HEOM approach

The main advantages are as follows: (i) the HEOM approach adopts a general form of the system Hamiltonian. It is applicable to a wide range of system parameters without additional derivation and programming efforts. The different transport processes can be handled in a unified manner and the transient dynamics can be studied readily; (ii) the HEOM approach is nonperturbative. It treats quantum impurity systems from the perspective of open dissipative dynamics. In principle, the HEOM formalism is formally accurate for noninteracting electron reservoirs. It also resolves non-perturbatively the combined effects of electron–electron (e–e) interactions; (iii) in HEOM all the system-bath correlations are taken into consideration. It is capable of characterizing both static and transient electronic properties of strongly correlated systems; and (iv) the HEOM is a high-accuracy numerical approach. It has the ability to achieve the same level of accuracy as the the numerical renormalization group (NRG) and quantum Monte Carlo approaches.

The disadvantages for HEOM approach are mainly shown as follows: (i) it can only deal with the case of finite temperatures, while the zero temperature is inaccessible; (ii) a higher truncation level is necessary to ensure numerical convergence at an extreme low temperature, this leading to a rapid growth of the required computational resources; (iii) the computation cost increases dramatically as the degree of system increases. For example, we can not reach the problem that a quintuple-impurity Anderson model with strong e–e interactions at present.

As a successful application, the HEOM approach has been proved to be capable of quantitatively describing the essential signatures of Kondo physics[33,39,46,48] and achieving the accuracy of the NRG approach. Currently for a typical Anderson model, the HEOM approach reaches quantitatively accuracy for temperature $T \geq 0.1T_{\mathrm{K}}$ (Kondo temperature). Here, we show the benchmark scaling character and spectral features of the Kondo effect in single-impurity Anderson model (SIAM). Figure A1 indicates the HEOM results exhibit the correct scaling behavior by Kondo temperature T_{K}. By re-

ferring to the calculated $\mathrm{d}I/\mathrm{d}V$ versus T/T_K as depicted in Fig. A1, the universal scaling is clearly manifested at $T < T_\mathrm{K}$ and $\Delta \ll U \ll W$ (where Δ is the hybrid function and W is the band width of itinerant electrons). It is clear at low temperature ($T < T_\mathrm{K}$), no matter of our parameters, the results of differential conductance fall on one line, which characters the Kondo effect. For unscaled T, we draw it in the inset (for more details, please refer to Ref. [39]).

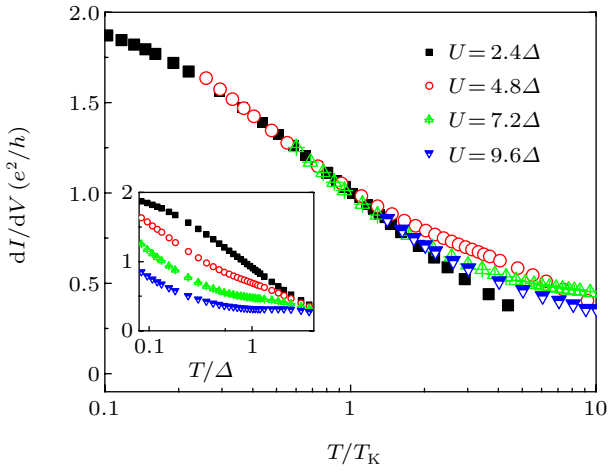


Fig. A1. The $\mathrm{d}I/\mathrm{d}V$ calculated by HEOM vs. T/T_K for symmetric SIAM. The inset depicts $\mathrm{d}I/\mathrm{d}V$ vs. unscaled T.

Figure A2 depicts the calculated $A(\omega)$ of a symmetric SIAM, from weak ($U = 0.5\pi\Delta$) to strong ($U = 6\pi\Delta$) e–e interactions. For comparison, we also show results obtained by using the full density matrix NRG method, where a self-energy scheme is employed, and the results are averaged over 8 different logarithmic discretization. Apparently, the two sets of curves agree quantitatively at all values of U studied. In the weak ($U = 0.5$ and $1.0\pi\Delta$) and intermediate ($U = 3\pi\Delta$) interaction regimes, HEOM and NRG curves almost overlap with each other; while in the strong ($U = 6\pi\Delta$) interaction regime minor deviation is observed in the height of Hubbard peaks (for more details, please refer to Ref. [39]).

As aforementioned, the HEOM approach has been applied to investigate the Kondo effect in different QD structures. For example, Ye *et al.* applied it onto two-level QDs with Kondo correlations, providing an understanding of, and a viable mechanism for controlling, the thermoelectric properties of strongly correlated QD systems.[53] In coupled double QDs, Li *et al.* studied the Kondo-peak splitting and resonance enhancement caused by inter-dot tunneling;[33] Cheng *et al.* investigated transport properties in the real-time domain;[54] and Pan *et al.* studied the Kondo effect in the context of ferromagnetic RKKY interaction.[55] Recently, in open triple QDs, Cheng *et al.* investigated the reappearance of the Kondo effect[45] and long-range overlapping of Kondo clouds.[48]

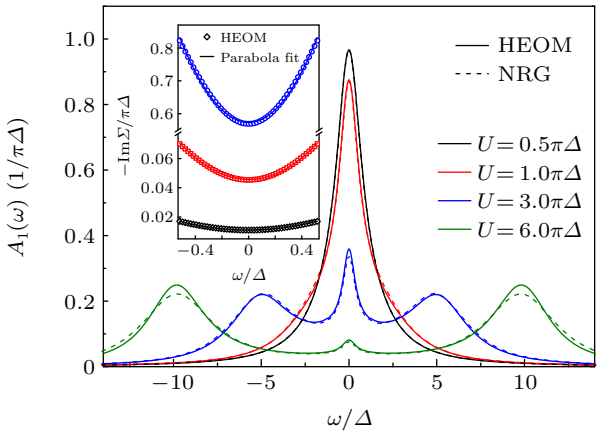


Fig. A2. Comparison between $A(\omega)$ of symmetric SIAM calculated by HEOM and NRG methods. The parameters adopted are $T = 0.2$ and $W = 50$ (in units of Δ). The inset shows the imaginary part of interaction self-energy calculated from HEOM at energy close to $\omega = 0$.

Appendix B: Some supplementary information about the physical image

Figure B1 depicts the spectral density functions $A_{1\uparrow}(\omega)$ in the absence of external magnetic field with the increase of tunneling strength t. The spectral density functions is shifting left with the increasing t, which means the electron–hole is asymmetry. And we can recover the symmetry of electron–hole by applied a perpendicular magnetic field to the TTQD structure. We adjust the flux at $\varphi = \pi/2$ with the increasing tunneling strength t in the right part of Fig. B1, and the electron–hole recover to symmetry.

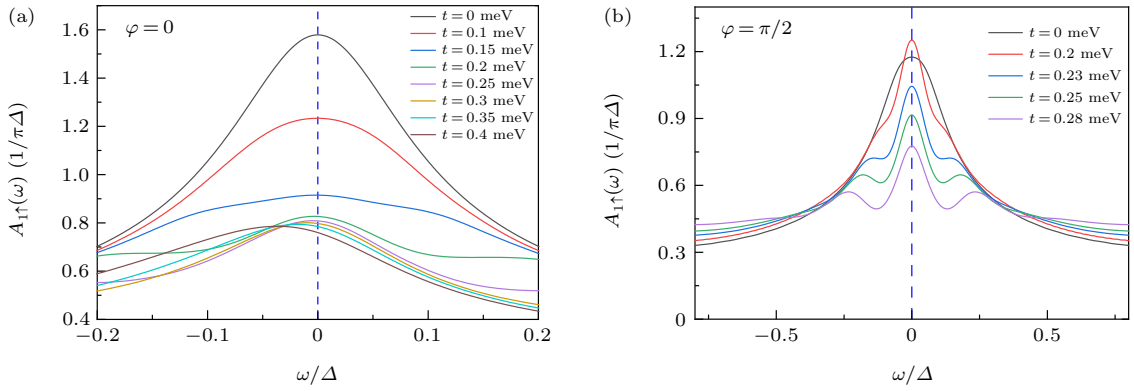


Fig. B1. (a) The $A_{1\uparrow}(\omega)$ as function of ω with the increase of t; and $A_1(\omega) = 2A_{1\uparrow}(\omega) = 2A_{1\downarrow}(\omega)$. (b) The $A_{1\uparrow}(\omega)$ calculated by HEOM versus ω/Δ with the flux $\varphi = \pi/2$.

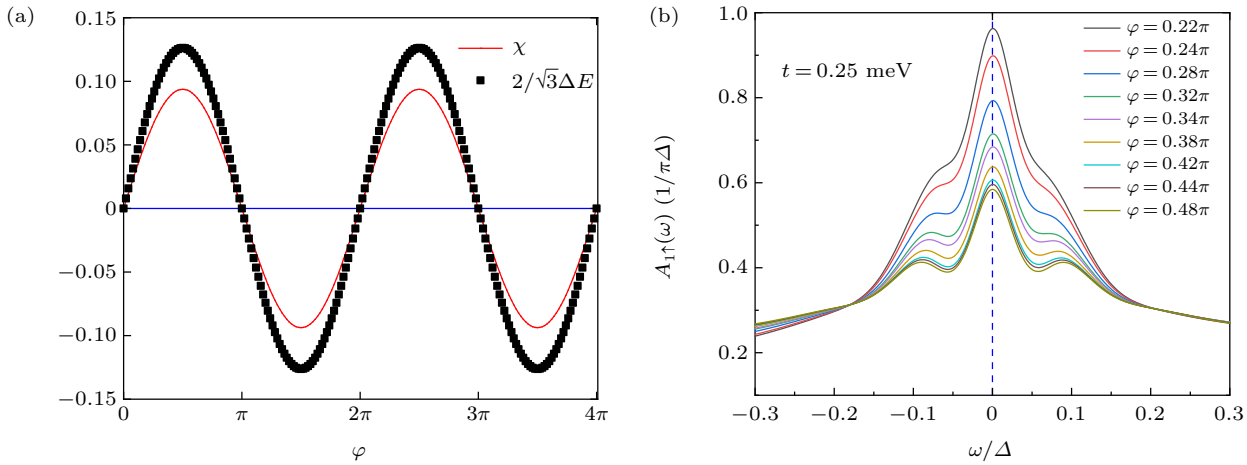


Fig. B2. (a) The χ and ΔE as function of φ in two periods. The dotted line in red denotes the theoretical deduce χ and the line in black is the numerical computation ΔE [we set $2/\sqrt{3}\Delta E$ for simplification]. (b) The $A_{1\uparrow}(\omega)$ as function of ω/Δ with the increase of flux φ; $A_1(\omega) = 2A_{1\uparrow}(\omega) = 2A_{1\downarrow}(\omega)$. We calculate at $t = 0.25$ meV.

The left part of Fig. B2 depicts the comparison for the numerical computation and theoretical deduce about distance between two lateral peaks [in Fig. 3(b) of the main text], which as function of the flux φ with a perpendicular magnetic field. The periodic variation of the curve with the flux φ is adjustable; the difference between two curves derives from the non-perturbation computing method. And the right part of Fig. B2 depicts the spectral density functions $A_{1\uparrow}(\omega)$ with the increase of flux φ in half period when applied perpendicular magnetic field to the TTQD structure. The lateral peaks is expanding with the increase of flux; and the distance between two lateral peaks is linear fitting well with the equation $\chi \sim 24t^3 \sin(\varphi)/U^2$.

Figure B3 depicts the spectral density functions $A(\omega)$ of QD1 with the increasing Zeeman magnetic field B in the absence of perpendicular magnetic field. With the increase of the Zeeman magnetic field B, the spectral density functions splits into two peaks, from Kondo resonance peak [in the Fig. 2(b) of main text], which means the splitting of spin freedom.

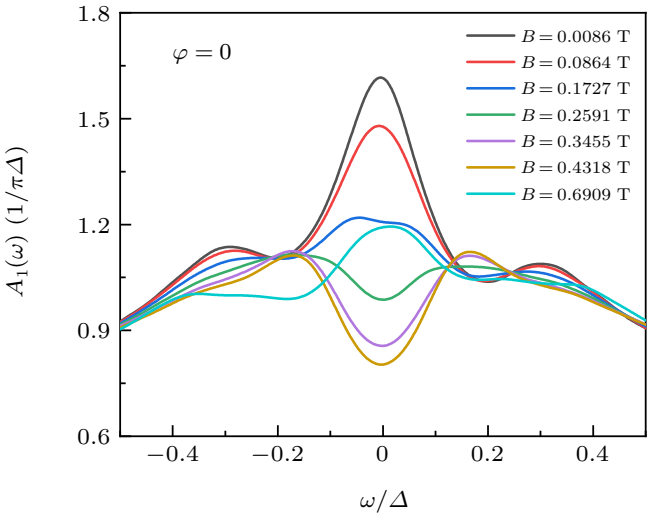


Fig. B3. The influence of Zeeman magnetic field without perpendicular field. $A_1(\omega)$ as function of ω/Δ with the increase of Zeeman magnetic field B.

References

[1] Berry M V 1984 *Proc. R. Soc. Lond. A* **392** 45
[2] Taguchi Y, Oohara Y, Yoshizawa H, Nagaosa N and Tokura Y 2001 *Science* **291** 2573
[3] Ohgushi K, Murakami S and Nagaosa N 2000 *Phys. Rev. B* **62** R6065
[4] Wen X G, Zee A and Wilczek F 1989 *Phys. Rev. B* **39** 11413
[5] Lee P A and Nagaosa N 1992 *Phys. Rev. B* **46** 5621
[6] Yang K, Warman L K and Girvin S M 1993 *Phys. Rev. Lett.* **70** 2641
[7] Kondo J 1964 *Prog. Theor. Phys.* **32** 37
[8] Hewson A C 1993 *The Kondo Problem to Heavy Fermions* (Cambridge: Cambridge University Press)
[9] Goldhaber-Gordon D, Shtrikman H, Mahalu D, Abusch-Magder D, Meirav U and Kastner M A 1998 *Nature* **391** 156
[10] Liang W J, Shores M P, Bockrath M, Long J R and Park H 2002 *Nature* **417** 725
[11] Nygard J, Cobden D H and Lindelof P E 2000 *Nature* **408** 342
[12] Costi T A 2000 *Phys. Rev. Lett.* **85** 1504
[13] Kuzmenko T, Kikoin K and Avishai Y 2006 *Phy. Rev. Lett.* **96** 046601
[14] Delgado F, Shim Y P, Korkusinski M and Hawrylak P 2007 *Phy. Rev. B* **76** 115332
[15] Numata T, Nisikawa Y, Oguri A and Hewson A C 2009 *Phy. Rev. B* **80** 155330
[16] Oguri A, Amaha S, Nishikawa Y, Numata T, Shimamoto M, Hewson A C and Tarucha S 2011 *Phy. Rev. B* **83** 205304
[17] Mitchell A K, Jarrold T F and Logan D E 2009 *Phys. Rev. B* **79** 085124
[18] Mitchell A K, Jarrold T F, Galpin M R and Logan D E 2013 *J. Phys. Chem. B* **117** 12777
[19] Kim C I, Kang C J, Choe M I, Yun C S and Ahn J K 2019 *Solid State Commun.* **289** 12
[20] Ingersent K, Ludwig A W W and Affleck I 2005 *Phys. Rev. Lett.* **95** 257204
[21] Žitko R and Bonča J 2008 *Phys. Rev. B* **77** 245112
[22] Mitchell A K and Logan D E 2010 *Phys. Rev. B* **81** 075126
[23] Tooski S B, Ramšak A and Bu/ka B R 2016 *Physica E* **75** 345
[24] Vernek E, Büsser C A, Martins G B, Anda E V, Sandler N and Ulloa S E 2009 *Phys. Rev. B* **80** 035119
[25] Koga M, Matsumoto M and Kusunose H 2012 *J. Phys. Soc. Jpn.* **81** 123703
[26] Tooski S B, Bu/ka B R, Žitko R and Ramšak A 2014 *Eur. Phys. J. B* **87** 145
[27] Yoo G, Park J, Lee S S B and Sim H S 2014 *Phys. Rev. Lett.* **113** 236601
[28] Koga M, Matsumoto M and Kusunose H 2016 *J. Phys. Soc. Jpn.* **85** 063702
[29] Scarola V W, Park K and Sarma S D 2004 *Phys. Rev. Lett.* **93** 120503
[30] Hsieh C Y, Rene A and Hawrylak P 2012 *Phys. Rev. B* **86** 115312
[31] Ye J, Kim Y B, Millis A J, Shraiman B I, Majumdar P and Tešanović Z 1999 *Phys. Rev. Lett.* **83** 3737
[32] Wang Y D, Zhu Z G, Wei J H and Yan Y J 2020 *Europhy. Lett.* **130** 17003

[33] Li Z H, Cheng Y X, Wei J H, Zheng X and Yan Y J 2018 *Phys. Rev. B* **98** 115133
[34] Aharonov Y and Bohm D 1959 *Phys. Rev.* **115** 485
[35] Hsieh C Y, Rene A and Hawrylak P 2012 *Phys. Rev. B* **86** 115312
[36] Jakub L and Bogdan R B 2014 *Phys. Rev. B* **90** 165427
[37] Jarillo-Herrero H P, Kong J, van der Zant H S J, Dekker C, Kouwenhoven L P and Franceschi S D 2005 *Nature* **434** 484
[38] Choi M S, López R and Aguado R 2005 *Phys. Rev. Lett.* **95** 067204
[39] Li Z H, Tong N H, Zheng X, Hou D, Wei J H, Hu J and Yan Y J 2012 *Phys. Rev. Lett.* **109** 266403
[40] Ye L Z, Wang X L, Hou D, Xu R X, Zheng X and Yan Y J 2016 *Wiley Interdisciplinary Reviews. Computational Molecular Science* **6** 608
[41] Feynman R P and Vernon F L 2000 *Annals of Physics* **281** 547
[42] Jin J S, Zheng X and Yan Y J 2008 *J. Chem. Phys.* **128** 234703
[43] Yan Y J 2014 *J. Chem. Phys.* **140** 054105
[44] Yan Y J, Jin J S, Xu R X and Zheng X 2016 *Front. Phys.* **11** 110306
[45] Cheng Y X, Wei J and Yan Y J 2015 *Europhy. Lett* **112** 57001
[46] Cheng Y X, Wang Y D, Wei J H, Zhu Z G and Yan Y J 2017 *Phys. Rev. B* **95** 155417
[47] Wang Y D, Ni J H and Wei J H 2017 *Phys. Rev. B* **96** 245426
[48] Cheng Y X, Wang Y D, Wei J H, Luo H G and Lin H Q 2019 *J. Phys.: Condens. Matter* **31** 155302
[49] Scarola V W and Sarma S D 2005 *Phys. Rev. A* **71** 032340
[50] Härtle R, Cohen G, Reichman D R and Millis A J 2013 *Phys. Rev. B* **88** 235426
[51] Härtle R and Millis A J 2013 *Phys. Rev. B* **90** 245426
[52] Okamoto J i, Mathey L and Härtle R 2016 *Phys. Rev. B* **94** 235411
[53] Ye L Z, Hou D, Wang R L, Cao D W, Zheng X and Yan Y J 2014 *Phys. Rev. B* **90** 165116
[54] Cheng Y X, Hou W J, Wang Y D, Li Z H, Wei J H and Yan Y J 2015 *New J. Phys.* **17**033009
[55] Pan L, Wang Y D, Li Z H, Wei J H and Yan Y J 2016 *J. Phys.: Condens. Matter* **29** 025601